ACS NANO

www.acsnano.org

ARTICLE

Exploring Mechanical Responses of Cells to Geometric Information Using Micropatterned DNA-Based Molecular Tension Probes

Feng Sun, Hongyun Li, Yuru Hu, Mengsheng Zhang, Wenxu Wang, Wei Chen,* and Zheng Liu*

Cite This: *ACS Nano* 2023, 17, 18584–18595

Read Online

ACCESS | Metrics & More | Article Recommendations | Supporting Information

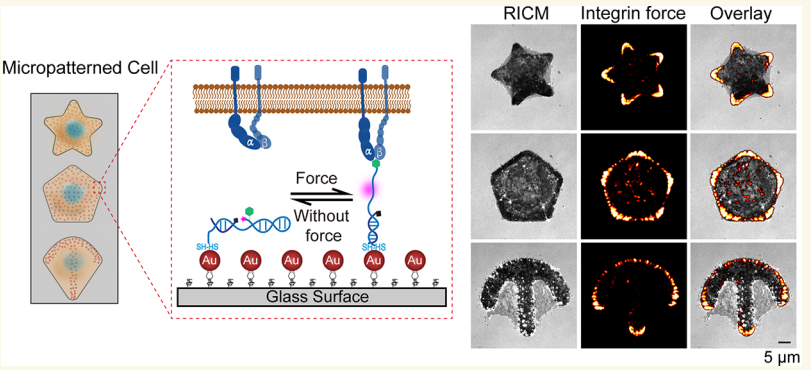

ABSTRACT: **The geometric shape of a cell is strongly influenced by the cytoskeleton, which, in turn, is regulated by integrin-mediated cell−extracellular matrix (ECM) interactions. To investigate the mechanical role of integrin in the geometrical interplay between cells and the ECM, we proposed a single-cell micropatterning technique combined with molecular tension fluorescence microscopy (MTFM), which allows us to characterize the mechanical properties of cells with prescribed geometries. Our results show that the curvature is a key geometric cue for cells to differentiate shapes in a membrane-tension- and actomyosin-dependent manner. Specifically, curvatures affect the size of focal adhesions (FAs) and induce a curvature-dependent density and spatial distribution of strong integrins. In addition, we found that the integrin subunit β_1 plays a critical role in the detection of geometric information. Overall, the integration of MTFM and single-cell micropatterning offers a robust approach for investigating the nexus between mechanical cues and cellular responses, holding potential for advancing our understanding of mechanobiology.**

KEYWORDS: *Integrin force, DNA-based tension probes, Cell geometry, Curvature, Mechanobiology*

INTRODUCTION

Cell geometry, with its attributes like shape and size, has a profound influence on a variety of cell functions, including but not limited to cell adhesion, proliferation, stem cell differentiation, and gene expression.[1−3] The cellular microenvironment *in situ*, as found within organs or tissues, is intricately structured and plays a pivotal role in dictating the cell structure, mechanics, polarity, and function.[4,5] However, in conventional cell culture settings, such as a culture dish, cells develop randomly with undefined geometry, which poses a challenge in studying the interplay between geometric information and cell behavior.

To overcome this predicament, researchers have extensively utilized various single-cell extracellular matrix (ECM) micropatterning methods to craft precise microscale patterns on cell culture substrates.[1,3,6−13] Using these geometrically controlled microenvironments, they have delved into different aspects of cellular physiology including cell adhesion, assembly of myosin and the cytoskeleton network, cell migration, and differentiation.[6,10,14−20]

Considering that cell geometry is largely influenced by the cytoskeleton, which is modulated by the integrin-mediated

Received: July 30, 2023
Accepted: September 13, 2023
Published: September 15, 2023

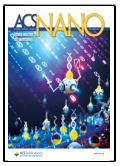

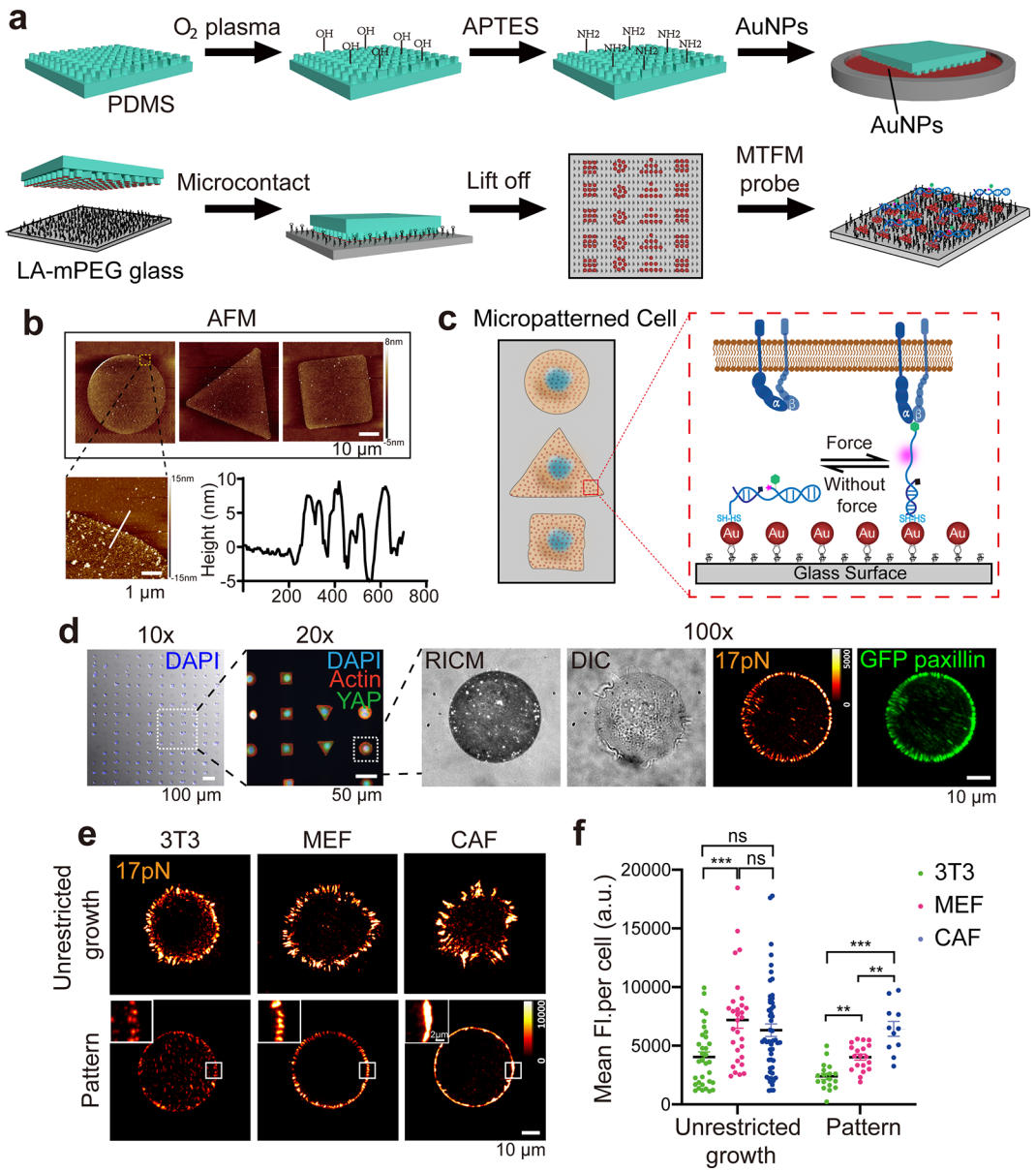

Figure 1. Fabrication and validation of micropatterned substrates with DNA-based tension probes. (a) Schematic depicting the fabrication process of substrates with micropatterned molecular tension probes. (b) 3D topography of Au NP patterns transferred to coverslips was measured by AFM. (c) Schematic illustrating the mechanism of RSDTP. (d) From left to right: MEFs spreading on the micropatterned substrates imaged using DIC with a 10× objective, immunofluorescent results of fixed MEFs on micropatterned substrates imaged using epifluorescence microscopes with a 20× objective (blue is DAPI, red is actin, green is YAP), GFP-paxillin MEF on circular micropatterns functionalized with 17 pN RSDTPs imaged using RICM, DIC, and TIRF with a 100× lens. (e) Representative TIRF images of 17 pN RSDTP signals for 3T3, MEF, and CAF cells on unrestricted glass and circular pattern substrates, and (f) corresponding statistical analysis of mean fluorescence intensity. Data are presented as mean values ± SEM from more than three independent experiments (for all shapes, number of cells >11). Ordinary one-way ANOVA tests were used to assess statistical significance (*$P < 0.001$, **$P < 0.01$, ns, not significant $P > 0.05$).**

mechanical interaction between the cell and ECM,[1,5,21] there has been a surge of interest in marrying cell mechanics measurement techniques with single-cell ECM micropatterning techniques. Researchers have dissected the responses of cells to geometric information from a viewpoint of mechanical force, thus shedding light on subtle mechanical differences that may be overlooked on unrestricted substrates.[7,22−24] This brought to the fore innovative techniques, such as those introduced by Fu et al., who established an elastic micropillar array that can regulate cell morphology and cell traction force, revealing a correlation between human mesenchymal stem cell (hMSC) morphology, early traction, and differentiation fate.[7] Subsequently, Han et al. used microcontact printing and micropillar arrays to control cell mechanics and adhesion parameters and found that the contractile force of cells can be regulated by a combination of substrate stiffness, spreading area, and pillar density.[22] By combining micropatterning with traction force microscopy (TFM), Oakes et al. reported that for a given pattern area, the work done by a cell on the substrate is closely related to the local curvature of the cell edge instead of the number of focal adhesions (FAs) or substrate stiffness.[23] In addition, Mandal et al. combined

https://doi.org/10.1021/acsnano.3c07088
ACS Nano 2023, 17, 18584−18595

micropatterning and optical tweezers to map the mechanical parameters of living cells and observed subtle mechanical parameter differences between nontumorigenic and metastatic cancer cells.[24] While these pioneering studies have significantly contributed to our understanding of cellular mechanics, certain limitations in techniques like TFM or elastic micropillar arrays can constrain our analyses. Specifically, their micrometer-level spatial resolution and nano- to sub-nN force sensitivity are not sufficient for probing the pN-level tensions transferred by integrins at the molecular scale. These constraints may limit the breadth and depth of our exploration of the interplay between cell mechanics and geometry.

On the other hand, a series of groundbreaking studies in the past decade have shown that molecular forces exerted on membrane receptors are essential for cellular mechanotransduction.[25−27] In particular, the development of molecular tension fluorescence microscopy (MTFM)[28] and its variants[29−37] has shown that it is capable of measuring molecular forces in living cells with high spatial resolution and pN force sensitivity and has revealed that these tiny forces can have a profound impact on processes such as T-cell receptor activation,[38−40] cell adhesion,[27,41−44] and Notch signaling.[27,45] However, in conventional MTFM experiments, cells grow in an unrestricted manner. This randomness can often obscure the finer nuances of different cell mechanics, making it challenging to discern these subtleties by using MTFM techniques alone. Here, we have developed a single-cell micropatterning technique combined with DNA-based MTFM probes, which allows for not only good control of cell shape and ECM microstructure but also accurate characterization of the mechanical transmission features in cell adhesion structures at the molecular level. By analyzing the tension signals on different micropatterns, we found a negative correlation between the cell area and the magnitude of the integrin force. More importantly, our results indicate that cells respond to the local curvature on the micropattern by adjusting not only the size of FAs but also the density and spatial distribution of mechanically strong integrins in a membrane-tension- and actomyosin-dependent manner. Finally, integrin subunit β_1 has been demonstrated to play a critical role in cell sensation of geometric information, possibly through fine-tuning the activity of ARP2/3 and the mechanical property of cell membrane. We believe this technique effectively exploits the advantages of the single-cell patterning method in regulating cell morphology with improved force sensitivity and spatial resolution of cell mechanics measurements.

RESULTS AND DISCUSSION

Fabrication of Substrates with Micropatterns Functionalized with DNA Tension Probes. To image the integrin tension of cells on micropatterns with MTFM probes, we propose a microcontact-printing-based immobilization method. This technique allows us to specifically modify the MTFM probes in the patterned region, as demonstrated in Figure 1a. In particular, we first fabricated a PDMS stamp with the desired micropatterns from a microfabricated Si mold, following the method outlined by the Bornens lab.[46] After treatment with oxygen plasma, the stamp was soaked in an APTES solution for amination modification, and 5 nm Au nanoparticles (NPs) were loaded onto the stamp via gold−nitrogen bonds. Our next step was to transfer Au NPs from PDMS to glass substrates, creating stronger Au−glass connections than the gold−nitrogen bonds between the Au NPs and the PDMS on the stamp. Specifically, plasma-treated coverslips were modified with lipoic acid following the procedure presented by the Salaita lab.[29,40] The PDMS stamp was then gently placed on the lipoic acid and mPEG functionalized glass and kept in a liquid environment overnight. As the gold−sulfur covalent bonds formed between the Au NPs and glass are stronger than the gold−nitrogen bonds, Au NPs were transferred to the coverslip after carefully removing the PDMS stamp the next day. This process resulted in the formation of micropatterns that replicated those on the stamp. The effectiveness and stability of this pattern transferring approach were further verified by atomic force microscopy (AFM) results. Here, intact patterns consistent with the designed 2D geometries and 5 nm in height, equivalent to the Au NP diameter, were observed (Figure 1b). Finally, after cleaning the glass substrate with ultrapure water, we incubated a drop of aqueous solution containing MTFM probes on the coverslip for 1 h. These steps allowed us to micropattern various molecular tension probes on the coverslip by using patterned Au NPs. To illustrate this, we used a recently developed DNA-based tension probe from our lab, the reversible shearing DNA-based tension probe (RSDTP).[47] RSDTP combines the reversibility of DNA hairpin probes[30,32] with the wide force range of tension gauge tether (TGT)[27] and can be used to measure integrin-mediated forces in living cells in a reversible and digital manner (Figures 1c and S1, Methods). Briefly, RSDTP mechanically unfolds when the cellular integrin force exceeds the design threshold of the DNA hairpin structure; it refolds when the integrin force falls below the structure's folding force. Thus, the combination of MTFM and the single-cell micropatterning method allows us to observe the spatial distribution and magnitude of integrin forces on these patterned cells through total internal reflection fluorescence (TIRF) microscopy as well as to study how the cell mechanics are modulated by different cell geometries.

To demonstrate the capability of the proposed method, we seeded mouse embryonic fibroblast (MEF) cells on a coverslip containing 17 pN RSDTP modified micropatterns. After 1 h of cell spreading, we observed that these cells selectively adhered to these micropatterns, indicating successful passivation in other areas. The specific adhesion results were clearly visible from the fluorescent staining results (Figures 1d and S2). Next, we collected the fluorescence signals of 17 pN RSDTPs and paxillin using TIRF microscopy. We also used the results of reflection interference contrast microscopy (RICM) and differential interference contrast microscopy (DIC) to validate the quality of the reported tension signals (Figure 1d). The results showed good overlap among the cell spreading area, Au NP patterns, and cell adhesion regions as indicated by DIC, RICM, and paxillin. Importantly, integrin tensions were reported with a high signal-to-noise ratio and well colocalized with paxillin at a spatial resolution close to the optical diffraction limit. After disrupting the actomyosin machinery using myosin II inhibitor (blebbistatin) or actin polymerization inhibitor (cytochalasin D, cytoD), a significant attenuation of the reported signals was observed (Figure S3), further demonstrating the fidelity of the reported signals.

We then sought to visualize the mechanical differences among fibroblast cells, including MEF cells, 3T3 cells, and cancer-associated fibroblast (CAF) cells (Figure 1e,f). Interestingly, while CAF cells displayed similar spatial characteristics and intensity of integrin tension to both MEF

https://doi.org/10.1021/acsnano.3c07088
ACS Nano 2023, 17, 18584−18595

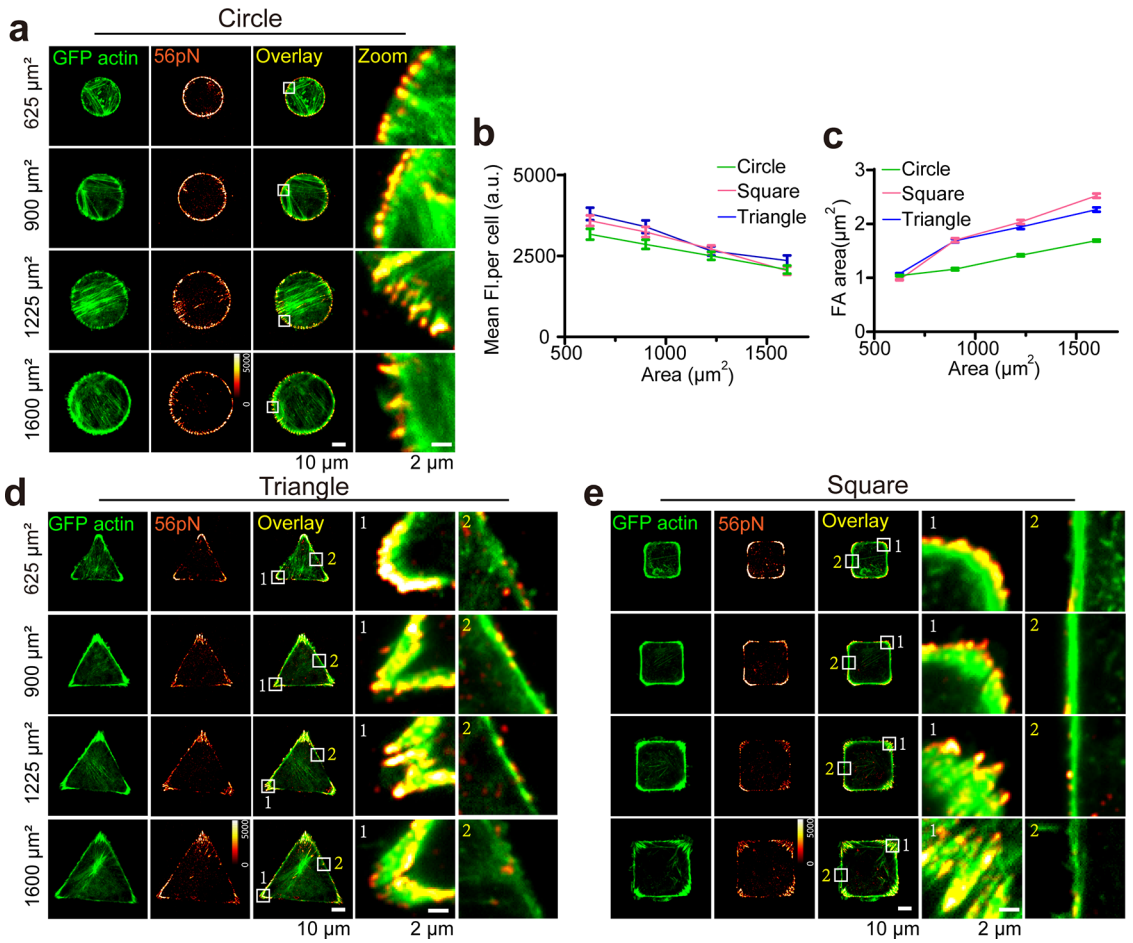

Figure 2. Relationship between cell mechanical force and micropattern area. Representative TIRF images of GFP-actin MEF cells on substrates with (a) circular, (d) triangular, and (e) square micropatterns of different size. Plots of (b) the average fluorescence intensity of 56 pN RSDTPs and (c) FA area as a function of pattern area (for each shape, number of cells >48). Data are presented as mean values ± SEM from more than three independent experiments.

cells and 3T3 cells when seeded on standard nonpatterned substrates, their mechanical differences were clearly visible when seeded on circular micropatterns. In particular, CAF cells showed continuous and tightly arranged loaded integrins encircling the pattern, clearly distinguishable from the dispersed signals of MEF and 3T3 cells (Figure 1e). The tension intensity of the CAF cells was also noticeably higher (Figure 1f). These results highlight the potential of MTFM-integrated micropatterns in detecting subtle mechanical discrepancies, which may facilitate the evaluation of mechanical homeostasis and interpretation of focal adhesion-mediated mechanotransduction in cells.

Correlation between Cell Mechanics and Geometry. In our previous study, we found that integrins capable of transmitting a strong force (>56 pN) are a minority in FAs but are critical for the stability of the FA structure in MEF.[47] Here, we used this highly mechanically stable probe, or 56 pN RSDTPs, to investigate the distribution of strong integrin force in cells with different geometries and the correlation between mean intensity and cell geometry conformation. We first functionalized circular patterns of different sizes (areas ranging from 625 to 1600 μm^2, Methods) with 56 pN RSDTPs. Note that the critical force for DNA probes varies with force loading rate and observation time scale;[48] therefore, the thresholds of RSDTPs we subsequently used (17, 56 pN) represent differences in mechanical stability of the DNA probes rather than the actual value transmitted by integrin in the experiments. After seeding GFP-actin-labeled MEFs on these patterns for 1 h, we collected the signals reported by the 56 pN RSDTPs and the fluorescent signals of actin using TIRF microscopy (Figure 2a and Supplementary Video). The results showed that the cell spreading area was well dictated by the pattern, with multiple stress fibers arching over the micropattern. Overall, integrin forces were evenly distributed along the circular edges. Interestingly, on the smaller circular micropatterns (<900 μm^2), the integrin forces were almost exclusively present in a punctate form at the tips of the stress fibers and were more evenly distributed between them, while the tension signal gradually shifted to a rod-like shape as the micropattern area increased, similar to what we have previously observed on unrestricted glass.[47] In addition, we found that the mean intensity of 56 pN RSDTP was significantly stronger on smaller patterns than on larger ones. To further analyze the relationship between the integrin force and spreading area, we calculated the integrated fluorescence intensity of the whole-cell tension signal and plotted it as a function of spreading area. The results showed a negative correlation between pattern area and mean fluorescence intensity, indicating that the proportion of strong integrin forces in cells decreased as the cell spread (Figure 2b). Interestingly, imaging paxillin (Figure S4), we found that FA size was positively correlated with spreading area (Figure 2c), suggesting that cells achieved a larger

https://doi.org/10.1021/acsnano.3c07088
ACS Nano 2023, 17, 18584−18595

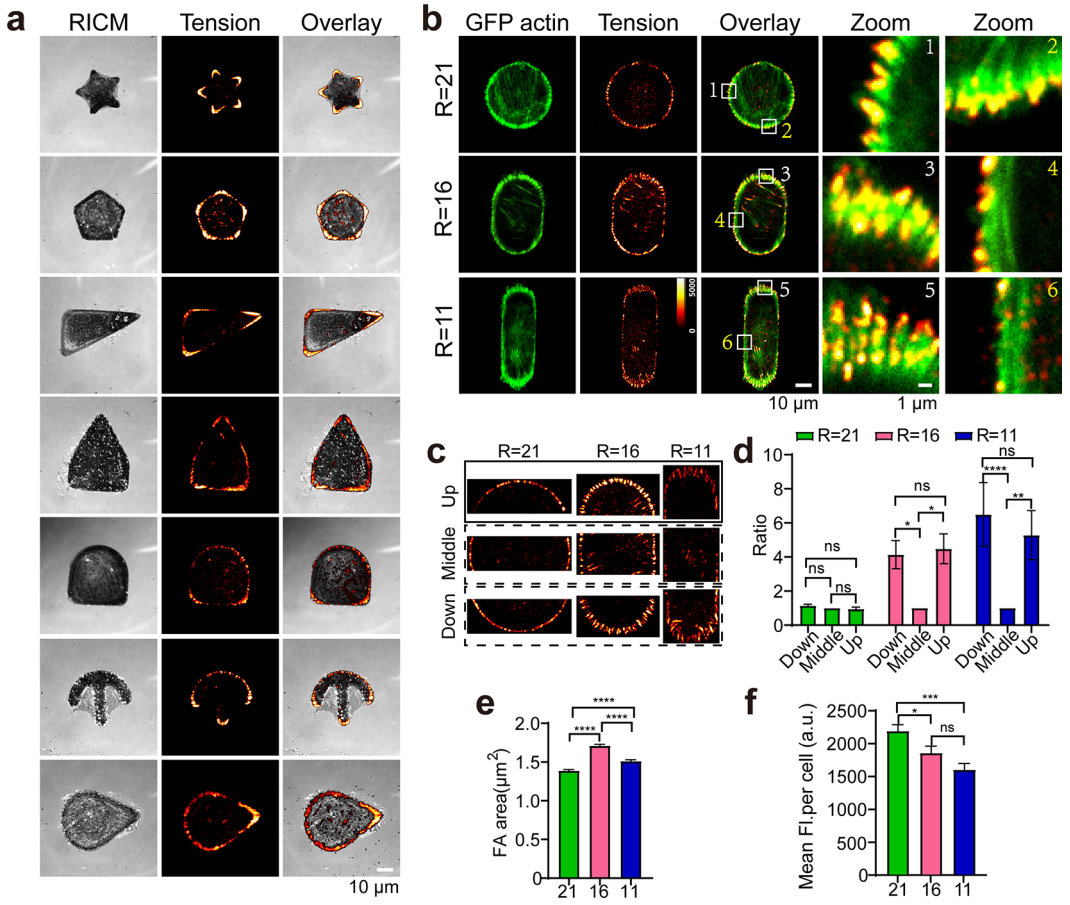

Figure 3. Effects of local curvature on the mechanical property of cells on micropatterns. (a) Representative RICM, TIRF, and overlay images of MEF on asymmetric patterns functionalized by 56 pN RSDTPs. (b) Representative TIRF images of MEF cells tagged with GFP-actin on substrates patterned with strips and circles of the same area (1400 μm^2) but different curvature. (c,d) Quantification of the inhomogeneity of tension signals using the ratio of average fluorescent intensity of tension signals in the "up" or "down" regions to that in the "middle" region (for each pattern, number of cells >30). Bar plots of (e) FA size and (f) mean fluorescent intensity of tension signals of cells on different micropatterns (for each pattern, number of cells >70). Data are presented as mean values ± SEM from more than three independent experiments. Ordinary one-way ANOVA tests were used to assess statistical significance (**P < 0.0001, ***P < 0.001, **P < 0.01, *P < 0.05, ns, not significant P > 0.05).**

spreading area by reducing the density of strong integrin forces in the FA.

Next, we prepared substrates consisting of micropatterns with the same area as the circular pattern but with a different shape (e.g., triangle and square) and repeated the aforementioned experiments (Figure 2d,e). Unlike the circular patterns, the forces of integrins in MEFs were mainly distributed in the corners of the triangles or squares, which is consistent with previous TFM observations.[49] Enlarged images of the different regions also showed that on triangular or square micropatterns, only very weak integrin forces were detected at the edges of the cells despite the presence of obvious stress fibers that maintain the cell shape. Statistical results showed that cells on circular, triangular, and square micropatterns maintained a similar trend in FA size and integrated fluorescence intensity of the tension signal relative to the pattern areas (Figure 2b,c). In addition, the spatial distribution of tension signals at the ends of stress fibers on triangular or square micropatterns was more heterogeneous than on circular micropatterns, and tension signals were significantly denser at corners (zoom 1 in Figure 2d,e) than along straight lines (zoom 2 in Figure 2d,e). These results suggest that cells modulate the distribution of integrin tension and the density of strong integrin forces to accommodate the complex ECM geometries, maintain stable FAs, and promote cell spreading.

Local Curvature Regulates the Magnitude and Spatial Distribution of Integrin Forces. Now that we have demonstrated that cells can modulate the spatial distribution of strong integrins on homogeneous and symmetric shapes like circles, squares, and equilateral triangles, we wondered whether this phenomenon would still be present when cells were seeded on arbitrary shapes like star patterns and scalene triangles. To test this, we first prepared seven different micropatterns functionalized with 56 pN RSDTPs following the aforementioned protocol and collected the signals of tension probes after MEFs were seeded for 1 h (Figure 3a). The results showed that the correlation between the cell shape and the spatial distribution of strong integrin forces remained present, and the force signals reported by 56 pN RSDTPs were clearly observed at the corners. Interestingly, we found that distinct spatial characteristics were observed between triangular and circular or rectangular and circular regions within the same pattern, suggesting that cells can modulate the integrin-mediated adhesion and mechanotransduction based on the local geometric information.

https://doi.org/10.1021/acsnano.3c07088
ACS Nano 2023, 17, 18584−18595

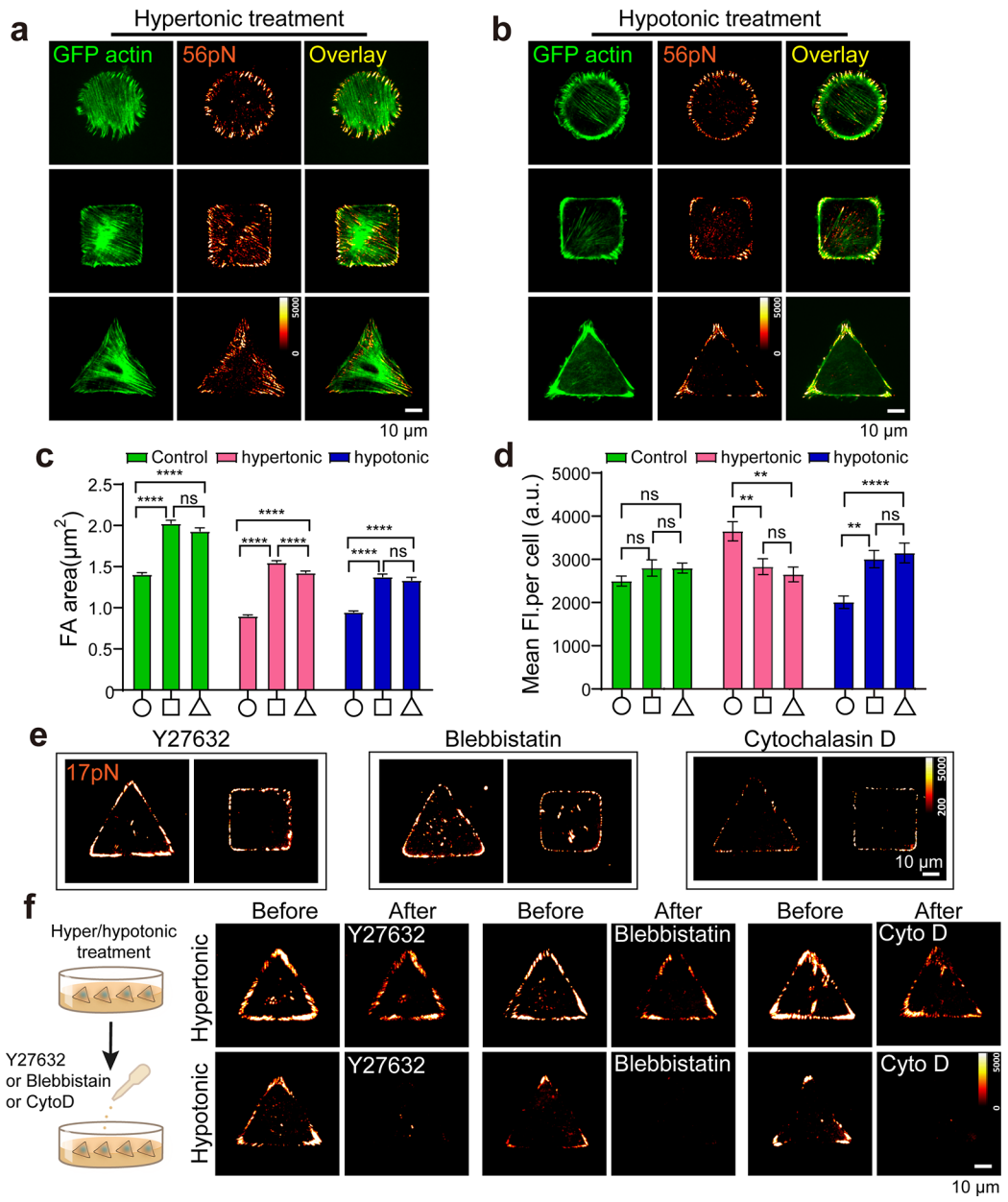

Figure 4. Regulation of cellular mechanical responses to local curvature by membrane tension and integrin-mediated molecular clutch. (a) Representative TIRF images of MEF cells tagged with GFP-actin after (a) hypertonic treatment or (b) hypotonic treatment. Bar plots of (c) FA size and (d) mean fluorescent intensity of tension signals of cells on different micropatterns with the same area (1225 μm^2) after hypertonic and hypotonic treatment (for each pattern, number of cells >29). (e) Representative TIRF images of 17 pN RSDTP signals of MEF after treatment with Y27632 (2 μM), blebbistatin (2 μM), and cytochalasin D (0.2 μM). (f) Representative TIRF images of MEFs after hypertonic or hypotonic treatment, followed by treatment with Y27632 (2 μM), blebbistatin (2 μM), and cytochalasin D (0.2 μM). Data are presented as mean values ± SEM from more than three independent experiments. Ordinary one-way ANOVA tests were used to assess statistical significance (****P < 0.0001, ***P < 0.001, **P < 0.01, *P < 0.05, ns, not significant P > 0.05).

To further understand how geometric shapes influence the spatial distribution of tension signals, we investigated the effect of geometrical properties of micropatterns other than the area on integrin tensions. We focused on the curvature as a parameter that differentiates circles from triangles and squares and defines the local geometry. To test this, we prepared substrates patterned with circles or strips with rounded ends. The area of all patterns was kept at 1400 μm^2, but the curvature radius for strips was either 16 or 11 μm at both ends, while the radius of the circle was 21 μm (Figure 3b). By comparing the spatial distribution of actin and tension signals of MEFs transfected with GFP-actin after 1 h of seeding, we observed a higher density of stress fibers at both ends of strips compared to circles, and mechanical forces colocalized with the stress fiber tips were also denser (zooms 3, 5 in Figure 3b), similar to the phenomenon observed in the literature using the TFM technique.[23] To quantify the uneven distribution of strong integrins, we calculated the average fluorescence intensity of the probe signals either at the ends or in the middle of the micropatterns, and their ratio was used to measure the inhomogeneity (Figure 3c). The results showed that unlike the uniformly distributed mechanical forces on the

https://doi.org/10.1021/acsnano.3c07088
ACS Nano 2023, 17, 18584−18595

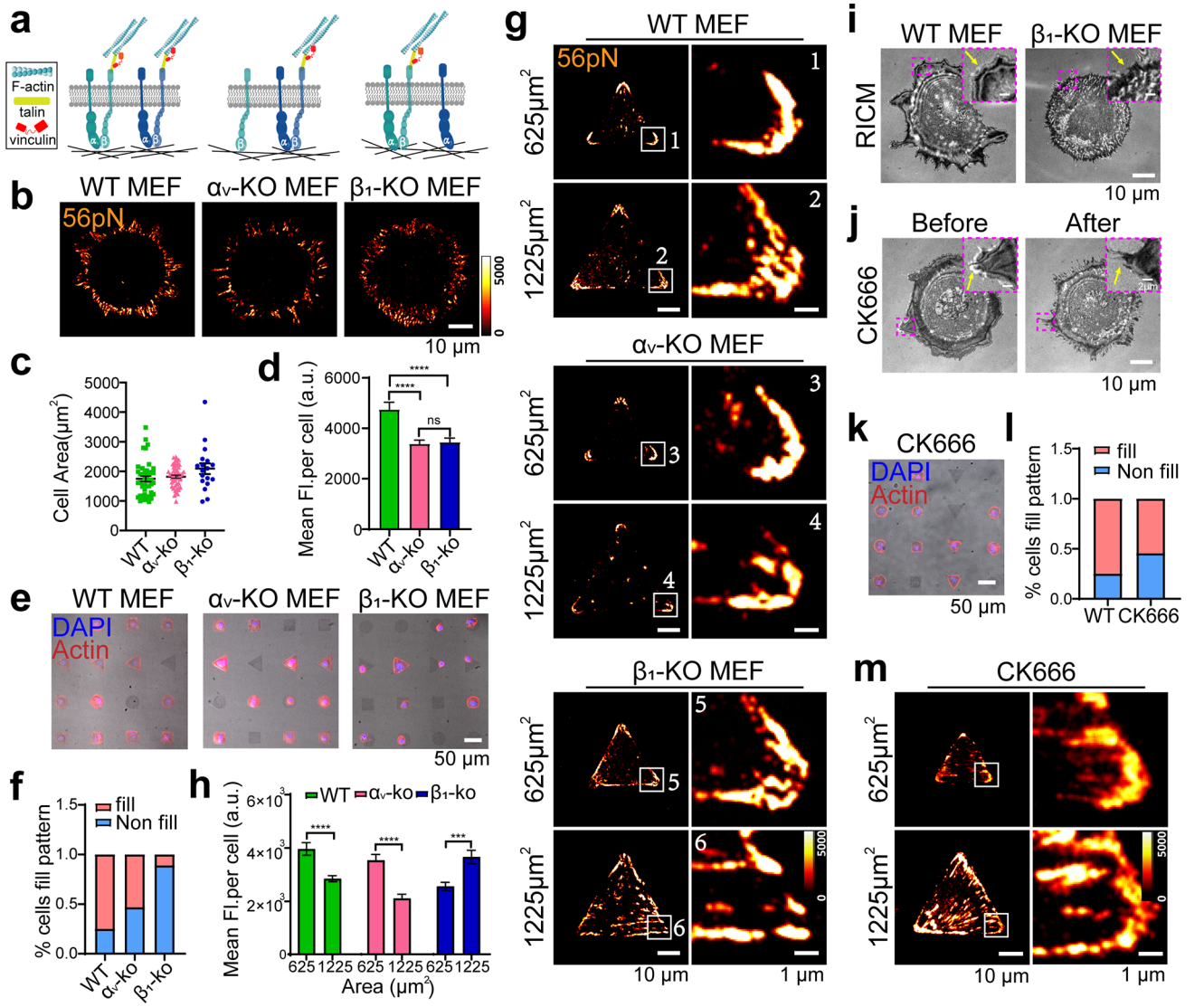

Figure 5. Effects of integrin subunits α_v and β_1 on mechanical responses of cells to geometry of micropatterns. (a) Schematic diagram of integrin-subunit-mediated mechanotransduction. (b) Representative TIRF images of WT MEF, α_v-KO MEF, and β_1-KO MEF seeded on an unrestricted substrate with 56 pN RSDTPs and (c) the corresponding statistical results of cell spreading area and (d) the corresponding mean fluorescence intensity of tension signals (for each type, number of cells >24). Data are mean values ± SEM from three independent experiments. Ordinary one-way ANOVA tests were used to assess statistical significance (****P < 0.0001, ns, not significant P > 0.05). (e) Immunofluorescent results of different fixed MEFs on micropatterned substrates of the same region (1225 μm^2) with a 20× objective (blue is DAPI, red is actin). From left to right: WT MEF, α_v-KO MEF, and β_1-KO MEF. (f) The statistical results of the proportion of a single cell covering the entire pattern in Figure e (for each type, number of cells >100). (g) Representative TIRF images of WT MEF, α_v-KO MEF, and β_1-KO MEF seeded on triangular micropatterns with 625 and 1225 μm^2 and (h) corresponding mean fluorescent intensity of tension signals (for each pattern, number of cells >42). Statistical comparisons were tested using an unpaired two-tailed Student's t test (****P < 0.0001, ***P < 0.001). (i) Representative RICM and zoom images of WT MEFs and β_1-KO MEFs. (j) Representative RICM images of WT MEFs before and after treatment with CK666. (k) Immunofluorescent results of fixed MEF cells pretreated with CK666 (150 μM) on micropatterned substrates of the same region (1225 μm^2) using a 20× objective (blue is DAPI, red is actin). (l) The statistical results of the proportion of a single cell covering the entire pattern after pretreated with CK666 (for each type, number of cells >100). (m) Representative TIRF images of WT MEF cells pretreated with CK666 seeded on triangular micropatterns with 625 and 1225 μm^2. Data are mean values ± SEM from three independent experiments.

circular pattern where the ratio was close to 1, the densities of highly loaded integrins at both ends of cells on strips were significantly different from that in the middle with the ratio much higher than 1. More importantly, the inhomogeneity of cells on rounder strips with a larger curvature radius was significantly lower than that with a smaller curvature radius (Figure 3d), implying that cells can sense local curvatures and adjust the spatial distribution of stress fibers and strong integrins. Interestingly, even with the same area, there were significant changes in FA size and the density of strong force-bearing integrins between these three micropatterns (Figure 3e,f), indicating that cells may respond to the local curvature of micropatterns through a complex cascade of responses in addition to the area.

Membrane Tension and Actomyosin Regulate the Response of Integrin-Mediated Adhesion to Geometry. Since membrane tension has been reported to be closely related to the shapes of cells,[50,51] we wondered whether it was

https://doi.org/10.1021/acsnano.3c07088
ACS Nano 2023, 17, 18584−18595

also involved in regulating the interaction between the local curvature of the ECM and cell mechanics. To test this, we first attempted to observe the mechanical responses of cells on micropatterned substrates with different shapes but equal areas (1225 μm^2) after manipulating the membrane tension through osmotic shock experiments. Specifically, after seeding for 1 h, MEF cells were treated with sucrose or 0.5× PBS for 30 min, and stress fibers and tension signals of the cells were recorded (Figure 4a,b). The results showed that altering the membrane tension through hypertonicity led to significant rearrangement of the cytoskeleton with smaller FAs and more actin bundles in the central regions of all three patterns (Figure 4a,c). The relationships between micropattern shape and tension signal intensity were also changed (Figures 4d and S5), and the uneven distribution on square and triangular micropatterns was weakened (Figures 4a and S5), suggesting the critical role of membrane tension in regulating the arrangement of integrin-mediated adhesion in response to geometric cues. Interestingly, after hypotonic treatment, the trends in mechanical properties, including mean fluorescence intensity and FA size, were similar to that before the treatment (Figures 4c,d and S6), and the inhomogeneous distribution of strong integrin forces on square and triangular micropatterns persisted (Figures 4b and S6). We speculate that these discrepancies between hypertonicity and hypotonicity may arise from their different effects on the membrane tension. For instance, the expansion of the membrane through hypotonic treatment increases global membrane tension but maintains the pattern of tension induced by local curvatures, while the contraction of the membrane through hypertonic treatment reduces global tension and eliminates local differences.

Next, as we have demonstrated the role of actomyosin in generating the integrin tension of cells seeded on micropatterns (Figure S3), we attempted to probe its effect on the spatial characteristics of integrin-mediated adhesion. To this end, we first observed the effects of Y27632 (2 μM), blebbistatin (2 μM), and cytochalasin D (0.2 μM) at a lower dose that would disturb actomyosin contractility or actin polymerization without completely inactivating integrins. As strong integrins were mostly inhibited after the treatment with these drugs, we replaced 56 pN RSDTPs with 17 pN RSDTPs to report integrin tension. We found that while the intensity of integrin tension was weakened, consistent with Figure S3, the spatial reorganization of integrin-mediated adhesion was distributed along the edge of the pattern rather than concentrating on the corners, which was clearly disturbed after the treatment (Figure 4e). These results indicate that actomyosin participates in regulating not only the strength but also the spatial organization of integrin-mediated adhesion during spreading on micropatterns.

Given that both membrane tension and actomyosin machinery have been identified to regulate the spatial characteristics of integrins, we wondered whether their effects were interconnected. To test this, we collected the tension signals of 17 pN RSDTPs after treating cells in hyper/hypotonic solution with Y27632, blebbistatin, and cytochalasin D at a low concentration. The results *in situ* showed that the spatial dependence of integrin-mediated adhesion on the local curvatures, disturbed in hypertonic solution, was not recovered by either drug, and the tension signals after all treatment were mostly attenuated, especially in hypotonic solution (Figures 4f and S7, and S8). Thus, we speculate that the spatial distribution of integrin-mediated adhesion was regulated by both membrane tension and actomyosin independently.

Taken together, our findings indicate that both membrane tension and actomyosin are crucial in regulating the mechanical response of cells to local curvature, likely through the interplay with the integrin-mediated molecular clutch. For example, higher membrane tension at the corners of micropatterns may lead to increased resistance during actin polymerization and enhance integrin recruitment to slow actin retrograde flow.[52] This may require further investigation through biophysical modeling.

β_1 Integrin Is Particularly Important in Sensing ECM Geometry. The $\alpha_5\beta_1$ and α_v-like integrins in MEF cells bind to RGD peptides in fibronectin to mediate cell adhesion and migration, and different types of integrins are assigned specific functions in these processes.[53,54] However, it is unclear whether these integrins have different functions in sensing geometric information. To investigate this, we disrupted cell−ECM interactions and observed the mechanical properties of cells on triangular micropatterns. Specifically, we created two cell lines with different cell−ECM interaction characteristics by knocking out integrin subunits α_v (α_v-KO MEF) or β_1 (β_1-KO MEF) using CRISPR/Cas9 (Figure S9). To verify their effects on cell−ECM interactions, we seeded both knockout and wild-type (WT) MEFs on unrestricted substrates modified with 56 pN RSDTPs for 1 h (Figure 5a,b). We found a slight difference in the spreading area of these cells (Figure 5c), which suggests that knockout of either α_v or β_1 does not affect normal adhesion and spreading on unrestricted substrates functionalized with RSDTPs. On the other hand, the statistical results of the mean fluorescence intensity showed a decreased force signal in knockout cells compared to WT (Figure 5d), consistent with reported effects of α_v and β_1 integrins on cellular traction.[53]

Next, we tested the effect of cell−ECM interactions on the recognition of geometric information in micropatterns by seeding β_1-KO MEFs, α_v-KO MEFs, and WT MEFs for 1 h on different patterns in the same area (1225 μm^2) modified with 56 pN RSDTPs before fixation (Figures 5e and S9). Surprisingly, the statistical results showed that while 53% of α_v-KO MEFs were still able to recognize the shape, slightly lower than that of WT MEFs (75%), only 11% of β_1-KO MEFs reached the corners of the pattern, staying only within the central region of the pattern (Figure 5f). This result suggests that the integrin subunit β_1 is critical for pattern shape recognition. To test whether cell mechanics are related to this regulatory role of integrin subunit β_1, we imaged the tension signals of the 56 pN RSDTPs of these three types of cells that completely covered the triangles. Interestingly, while the tension signals of WT MEFs and α_v-KO MEFs decreased with increasing area, the opposite trend was observed in β_1-KO MEFs (Figure 5g,h). Furthermore, when β_1-KO MEF cells were spread over the pattern, the mechanical signal was not confined to the vertexes of the triangle. Instead, a significant amount of strong integrins was observed along the sides or inside the triangles, especially in larger triangle. A similar change in the spatial distribution of cellular force was also observed in β_1-KO MEFs seeded in square patterns (Figure S10) and mouse myoblast cells (C2C12) with β_1 integrins knocked down using shRNA (Figures S11, S12).

Since our results have demonstrated the critical role of membrane tension in the spatial pattern of integrin-mediated adhesion, we wondered whether β_1 integrin mediates the

https://doi.org/10.1021/acsnano.3c07088
ACS Nano 2023, 17, 18584−18595

sensation of geometric information through regulating the mechanical properties of the membrane. To test this, we initially observed the morphology of lamellipodia using RICM, and the results demonstrated a reduction in the lamellipodial size in β_1-KO cells compared to both WT and α_v-KO cells (Figures 5i and S13). This result is consistent with the known dynamics of β_1 integrin during cell spreading, where it preferentially localizes to the leading edge, including lamellipodia and membrane ruffles.[55] We speculate that this disturbance could hinder cells from navigating through the ECM landscape. For instance, the narrow lamellipodia may stop cells from exploring regions with a small radius of curvature, as we observed in β_1-KO cells.

Next, we attempted to identify the cytoskeleton adaptor protein involved in this β_1 integrin-membrane-geometric sensation pathway. Since ARP2/3 was reported to be a key player in actin branching that is regulated by β_1 integrin instead of α_v integrin,[53] we seeded MEFs that were pretreated with CK666 to inhibit ARP2/3 on flat substrates as well as micropatterned substrates and compared the morphology and reported tension signals to that of control cells. The results showed that, consistent with the existing report,[56] the lamellipodia of cells seeded on flat substrates were significantly inhibited after the treatment of CK666, similar to that in β_1-KO cells (Figure 5j). More importantly, even though the spreading area of MEFs was not affected by the treatment of CK666, the capability of cells to fill the patterns and the spatial patterns of strong integrins was clearly interrupted (Figure 5k–m). These results prompt us to hypothesize that the knockout of the β_1 integrin could inhibit the activity of ARP2/3, resulting in disordered membrane properties and associated sensation of geometric cues.

CONCLUSIONS

Measurements of cell mechanics at the molecular level, in particular, integrin-mediated force measurements, can provide insights into the physical interaction between cells and the microenvironment and the molecular mechanisms underlying these interactions. In this paper, we develop a combination of MTFM and ECM micropatterning to probe the cellular response to geometrical information from the perspective of mechanical forces.

We discovered that curvature is a crucial geometric cue for cells to distinguish between shapes, such as circles, triangles, and squares. This process is dependent on the membrane tension and actomyosin. Our results demonstrate that curvature not only affects the size of FAs but also induces a curvature-dependent density and spatial distribution of strong force-bearing integrins. Specifically, the density of these mechanically robust integrins is significantly higher in areas of greater curvature, leading to a difference in their spatial distribution on circles, triangles, or squares. This differential distribution and density of mechanically strong integrins add further dimensions for exploring the relationship between cell shape and physiological function. For instance, the high density of mechanically robust integrins in the corners of cells seeded on triangles or squares may promote stronger integrin-mediated downstream signaling, offering a fascinating approach to explore the interplay between cell shape and integrin-dependent processes, such as proliferation and differentiation. Importantly, the interplay between membrane tension and corner sensing could be utilized to fine-tune the cellular microenvironment for applications in tissue engineering and regenerative medicine. By adjusting the geometric features of the ECM, we could potentially manipulate integrin-mediated mechanotransduction to guide cell behavior, influencing processes, such as stem cell differentiation, tissue organization, and wound healing. Moreover, we have demonstrated the specific involvement of the integrin subunit β_1 in the sensation of ECM geometry, in which ARP2/3 has been further identified as a key component.

Looking ahead, the technique can be further extended by modifying other DNA-based probes. For instance, by replacing RSDTPs with TGTs that perturb integrin–ligand interaction once the transmitted forces exceed its designed thresholds,[27] we found the corners of micropattern were rarely filled, indicating the significance of intact integrin–ligand interaction in processing local geometrical information like curvatures (Figure S14). In addition, it can be seamlessly integrated with multiwell plates[57] to overcome the contradiction between the rich molecular information provided by MTFM experiments and their low throughput, which can potentially be applied to the screening of drug targets related to cell mechanics.[58] Overall, the combination of MTFM and cell micropatterning techniques could provide a powerful tool for investigating the relationship between mechanical cues and cellular responses, enabling discoveries and advances in the field of mechanobiology.

METHODS

Cell Culture and Transfection. Mouse embryonic fibroblasts (MEF) were maintained in Dulbecco's modified Eagle's Medium (DMEM) supplemented with 10% fetal bovine serum, HEPES (9.9 mM, Sigma), sodium pyruvate (1 mM), L-glutamine amide (2.1 mM), penicillin G (100 IU/mL), and streptomycin (100 μg/mL) and incubated at 37 °C with 5% CO_2. α_v-KO MEF and β_1-KO MEF cell lines were constructed in our laboratory by using CRISPR-Cas9. Briefly, the selected DNA sequences (target sequences 1:5′-tggagtttaagtcccaccag-3′ for subunit α_v and target sequences 2:5′-aatgtcaccaatcgcagcaa-3′ for β_1 integrin) were designed and cloned into PX459- CPISRP/Cas 9 Plasmid gifted by Prof. Kai Jiang at Wuhan University. Sh β_1 MEF and sh β_1 C2C12 cell lines were constructed in our lab using shRNA (5′- agatgaggttcaatttgaaat-3′ cloned into pLKO.1 vector). All transfections were carried out using the Lipofectamine 3000 Transfection Reagent (Invitrogen), following the standard protocols provided by Life Technologies.

Preparation of Molecular Tension Probes. Reversible DNA hairpins, or RSDTPs, unfold when the applied force is beyond the designed threshold and refold when the force is reduced. Irreversible DNA duplexes or TGTs rupture when the transmitted forces exceed the designed threshold. The threshold of both RSDTP and TGT can be adjusted from 4 to 60 pN by altering the positions of functional peptides such as cRGD (cyclic Arg-Gly-Asp), leading to a wide range of force threshold. This is because changes in the position of the applied force cause a shift in the unfolding mode between unzipping, mixed, and shearing. The RSDTPs employed in this study have structures and sequences that were previously established by our lab,[47] and the TGTs were slightly modified from the original ones described by the Ha Lab[27] in order to be covalently attached to Au NPs (Figure S1).

Micropatterning of DNA Probes Using Microcontact Printing. A Si master mold with desired geometric features was first fabricated via photolithography following the process developed by the Bornens lab.[46] The maximum size of the pattern is chosen based on the spreading area of MEFs after seeded on glass substrate for 1 h, and the minimum area is determined by the minimum size of the stamp that we can fabricate with our microfabrication facility. After the degassed mixture (10:1) of PDMS prepolymer and curing agent (Dow Corning) was poured into the mold and cured at 80 °C for 2 h, the cross-linked PDMS layer was peeled off and carefully cut

https://doi.org/10.1021/acsnano.3c07088
ACS Nano 2023, 17, 18584–18595

into multiple small stamps. Next, the stamp was activated in the oxygen plasma chamber for 3 min (30 s.c.c.m., 300 mTorr) and incubated with a 1% v/v (3-aminopropyl) triethoxysilane (Sigma-Aldrich) in ethanol for 1 h for amination. After being washed with ethanol two times, the stamp was dried with nitrogen and heated in an oven for 1 h at 80 °C to stabilize the functionalized amino groups. The stamp was then soaked in Au NP solution, which was synthesized using the method described by Piella et al.,[59] at 4 °C overnight and washed with nanopure water. Subsequentially, a coverslip was passivated and functionalized with lipo-acid following the procedures developed by the Salaita lab[40] prior to the gentle placement of the PDMS stamp on its center at 4 °C overnight. After the removal of the stamp, 10 μL of DNA tension probe solutions (50 nM) was added onto the coverslip and incubated at room temperature for 1 h. Finally, these functionalized coverslips were rinsed with PBS solution to remove nonspecifically bound probes.

Fluorescence Immunostaining. Cells were fixed and permeabilized with 4% PFA and 0.2% Triton X-100 (Sigma) in PBS for 10 min at room temperature. After being rinsed three times in warm PBS, fixed cells were blocked using 3% BSA for 1 h at room temperature and washed with PBS three times. To label F-actin, the prepared samples were incubated with 1 μg/mL phalloidin-TRITC (Solarbio) for 1 h at room temperature. A 1:200 dilution of mouse monoclonal anti-YAP (Santa Cruz Biotechnology) and a 1:200 dilution of Alexa-Fluor-488-conjugated goat antimouse IgG (Sangon Biotech) were used as primary and secondary antibodies for immunostaining of YAP following the protocol provided by the manufacture, respectively. Also, nuclei were labeled by incubating cells with 5 μg/mL DAPI (Sangon Biotech) for 10 min. Finally, all of the stained specimens were rinsed extensively with PBS, prior to microscopic observations.

AFM Measurement. The surface topography of the micropatterned samples was characterized by AFM (BioScope Resolve, Bruker) in ScanAsyst Air mode with ScanAsyst Air probes. All results were processed and rendered by using NanoScope Analysis (Bruker).

Cell Experiments. Functionalized coverslips were first assembled into cell imaging chambers (Thermo Fisher). After cell seeding, the chambers were placed in an incubator (37 °C, 5% CO_2, 95% humidity) to allow cell spreading. Imaging was performed using a Nikon Eclipse Ti2 inverted microscope with Nikon LU-N4 laser units, a stage top chamber (Okolab) for live-cell imaging and an EMCCD camera (ANDOR).

Imaging Processing and Statistical Analysis. Images were processed by using ImageJ and MATLAB software. All statistical data were derived from at least three independent experiments by using GraphPad Prism 9 or MATLAB software. Data are presented as the mean ± SEM. Two-tailed Student's t tests and ordinary one-way ANOVA tests were carried out to determine statistical significance between two cases and within more cases, respectively.

ASSOCIATED CONTENT

Supporting Information

The Supporting Information is available free of charge at https://pubs.acs.org/doi/10.1021/acsnano.3c07088.

Structure of RSDTP and TGT; investigation into the effects of cell shapes on YAP translocation; validation studies for tension signals on various micropatterns; tension mapping for MEFs under multiple conditions including hypertonic and hypotonic treatments; responses of sucrose-exposed and 0.5× PBS-treated MEFs to actomyosin-related drugs; comparative studies on the role of α_v and β_1 integrins in regulating the mechanical properties and spreading behaviors of MEFs and C2C12 cells; assessment of Arp2/3, α_v, and β_1 integrins' influence on actin structures in MEFs seeded on glass substrates; exploration into the effects of stable strong integrins on the sensation of geometric information by MEFs (PDF)

Supplementary Video: Simultaneous imaging of F-actin and molecular integrin tension on different micropatterns functionalized with 56 pN RSDTPs. The total imaging time is 95 min (AVI)

AUTHOR INFORMATION

Corresponding Authors

Zheng Liu − *TaiKang Center for Life and Medical Sciences, the Institute for Advanced Studies, Wuhan University, Wuhan 430072, China*; orcid.org/0000-0002-4252-4617; Email: zheng.liu@whu.edu.cn

Wei Chen − *TaiKang Center for Life and Medical Sciences, the Institute for Advanced Studies, Wuhan University, Wuhan 430072, China*; Email: w.chen@whu.edu.cn

Authors

Feng Sun − *TaiKang Center for Life and Medical Sciences, the Institute for Advanced Studies, Wuhan University, Wuhan 430072, China*

Hongyun Li − *TaiKang Center for Life and Medical Sciences, the Institute for Advanced Studies, Wuhan University, Wuhan 430072, China*

Yuru Hu − *TaiKang Center for Life and Medical Sciences, the Institute for Advanced Studies, Wuhan University, Wuhan 430072, China*

Mengsheng Zhang − *TaiKang Center for Life and Medical Sciences, the Institute for Advanced Studies, Wuhan University, Wuhan 430072, China*

Wenxu Wang − *TaiKang Center for Life and Medical Sciences, the Institute for Advanced Studies, Wuhan University, Wuhan 430072, China*

Complete contact information is available at: https://pubs.acs.org/10.1021/acsnano.3c07088

Author Contributions

Z.L. and W.C. conceived the project and directed the research. F.S. designed and performed the overall experiments and analyzed the data with the help of H.L., W.C., Y.H, M.Z., and W.W. F.S., W.C., and Z.L. wrote the paper.

Notes

The authors declare no competing financial interest.

ACKNOWLEDGMENTS

This work was supported by the National Natural Science Foundation of China (21775115, 32150016, 32071305), the Fundamental Research Funds for the Central Universities (2042021kf0030), and Innovation Funds for Postdocs in Hubei Province.

REFERENCES

(1) Chen, C. S.; Mrksich, M.; Huang, S.; Whitesides, G. M.; Ingber, D. E. Geometric control of cell life and death. *Science.* **1997**, *276* (5317), 1425−1428.

(2) Nelson, C. M.; Jean, R. P.; Tan, J. L.; Liu, W. F.; Sniadecki, N. J.; Spector, A. A.; Chen, C. S. Emergent patterns of growth controlled by multicellular form and mechanics. *Proc. Natl. Acad. Sci. U. S. A.* **2005**, *102* (33), 11594−11599.

(3) McBeath, R.; Pirone, D. M.; Nelson, C. M.; Bhadriraju, K.; Chen, C. S. Cell shape, cytoskeletal tension, and RhoA regulate stem cell lineage commitment. *Dev. Cell.* **2004**, *6* (4), 483−495.

(4) Mongera, A.; Pochitaloff, M.; Gustafson, H. J.; Stooke-Vaughan, G. A.; Rowghanian, P.; Kim, S.; Campàs, O. Mechanics of the cellular microenvironment as probed by cells in vivo during zebrafish

presomitic mesoderm differentiation. *Nat. Mater.* **2023**, *22* (1), 135−143.
(5) Mammoto, T.; Mammoto, A.; Ingber, D. E. Mechanobiology and Developmental Control. *Annu. Rev. Cell. Dev. Biol.* **2013**, *29* (1), 27−61.
(6) Thery, M. Micropatterning as a tool to decipher cell morphogenesis and functions. *J. Cell Sci.* **2010**, *123* (24), 4201−4213.
(7) Fu, J.; Wang, Y. K.; Yang, M. T.; Desai, R. A.; Yu, X.; Liu, Z.; Chen, C. S. Mechanical regulation of cell function with geometrically modulated elastomeric substrates. *Nat. Methods.* **2010**, *7* (9), 733−736.
(8) Singhvi, R.; Kumar, A.; Lopez, G. P.; Stephanopoulos, G. N.; Wang, D. I.; Whitesides, G. M.; Ingber, D. E. Engineering cell shape and function. *Science.* **1994**, *264* (5159), 696−698.
(9) Strale, P. O.; Azioune, A.; Bugnicourt, G.; Lecomte, Y.; Chahid, M.; Studer, V. Multiprotein Printing by Light-Induced Molecular Adsorption. *Adv. Mater.* **2016**, *28* (10), 2024−2029.
(10) Falconnet, D.; Csucs, G.; Grandin, H. M.; Textor, M. Surface engineering approaches to micropattern surfaces for cell-based assays. *Biomaterials.* **2006**, *27* (16), 3044−3063.
(11) Sarker, B.; Walter, C.; Pathak, A. Direct Micropatterning of Extracellular Matrix Proteins on Functionalized Polyacrylamide Hydrogels Shows Geometric Regulation of Cell−Cell Junctions. *ACS. Biomater. Sci. Eng.* **2018**, *4* (7), 2340−2349.
(12) Geiger, B.; Spatz, J. P.; Bershadsky, A. D. Environmental Sensing through Focal Adhesions. *Nat. Rev. Mol. Cell Biol.* **2009**, *10* (1), 21−33.
(13) Huang, J.; Grater, S. V.; Corbellini, F.; Rinck, S.; Bock, E.; Kemkemer, R.; Kessler, H.; Ding, J.; Spatz, J. P. Impact of Order and Disorder in Rgd Nanopatterns on Cell Adhesion. *Nano Lett.* **2009**, *9* (3), 1111−1116.
(14) Tee, Y. H.; Shemesh, T.; Thiagarajan, V.; Hariadi, R. F.; Anderson, K. L.; Page, C.; Volkmann, N.; Hanein, D.; Sivaramakrishnan, S.; Kozlov, M. M.; Bershadsky, A. D. Cellular chirality arising from the self-organization of the actin cytoskeleton. *Nat. Cell Biol.* **2015**, *17* (4), 445−457.
(15) Nahmias, Y.; Odde, D. J. Micropatterning of living cells by laser-guided direct writing: application to fabrication of hepatic-endothelial sinusoid-like structures. *Nat. Protoc.* **2006**, *1* (5), 2288−2296.
(16) Brückner, D. B.; Fink, A.; Schreiber, C.; Röttgermann, P. J. F.; Rädler, J. O.; Broedersz, C. P. Stochastic nonlinear dynamics of confined cell migration in two-state systems. *Nat. Phys.* **2019**, *15* (6), 595−601.
(17) Connelly, J. T.; Gautrot, J. E.; Trappmann, B.; Tan, D. W.; Donati, G.; Huck, W. T.; Watt, F. M. Actin and serum response factor transduce physical cues from the microenvironment to regulate epidermal stem cell fate decisions. *Nat. Cell Biol.* **2010**, *12* (7), 711−718.
(18) Thery, M.; Racine, V.; Pepin, A.; Piel, M.; Chen, Y.; Sibarita, J. B.; Bornens, M. The extracellular matrix guides the orientation of the cell division axis. *Nat. Cell Biol.* **2005**, *7* (10), 947−953.
(19) Cabezas, M. D.; Meckes, B.; Mirkin, C. A.; Mrksich, M. Subcellular Control over Focal Adhesion Anisotropy, Independent of Cell Morphology, Dictates Stem Cell Fate. *ACS Nano* **2019**, *13* (10), 11144−11152.
(20) Selhuber-Unkel, C.; Erdmann, T.; Lopez-Garcia, M.; Kessler, H.; Schwarz, U. S.; Spatz, J. P. Cell Adhesion Strength Is Controlled by Intermolecular Spacing of Adhesion Receptors. *Biophys. J.* **2010**, *98* (4), 543−551.
(21) Ron, A.; Azeloglu, E. U.; Calizo, R. C.; Hu, M. F.; Bhattacharya, S.; Chen, Y. B.; Jayaraman, G.; Lee, S.; Neves-Zaph, S. R.; Li, H.; Gordon, R. E.; He, J. C.; Hone, J. C.; Iyengar, R. Cell shape information is transduced through tension-independent mechanisms. *Nat. Commun.* **2017**, *8* (1), 2145.
(22) Han, S. J.; Bielawski, K. S.; Ting, L. H.; Rodriguez, M. L.; Sniadecki, N. J. Decoupling substrate stiffness, spread area, and micropost density: a close spatial relationship between traction forces and focal adhesions. *Biophys. J.* **2012**, *103* (4), 640−648.
(23) Oakes, P. W.; Banerjee, S.; Marchetti, M. C.; Gardel, M. L. Geometry regulates traction stresses in adherent cells. *Biophys. J.* **2014**, *107* (4), 825−833.
(24) Mandal, K.; Asnacios, A.; Goud, B.; Manneville, J. B. Mapping intracellular mechanics on micropatterned substrates. *Proc. Natl. Acad. Sci. U. S. A.* **2016**, *113* (46), E7159−E7168.
(25) Liu, Y.; Galior, K.; Ma, V. P. Y.; Salaita, K. Molecular Tension Probes for Imaging Forces at the Cell Surface. *Acc. Chem. Res.* **2017**, *50* (12), 2915−2924.
(26) Ma, V. P.Y.; Salaita, K. DNA Nanotechnology as an Emerging Tool to Study Mechanotransduction in Living Systems. *Small.* **2019**, *15* (26), 1900961.
(27) Wang, X.; Ha, T. Defining single molecular forces required to activate integrin and notch signaling. *Science.* **2013**, *340* (6135), 991−994.
(28) Stabley, D. R.; Jurchenko, C.; Marshall, S. S.; Salaita, K. S. Visualizing mechanical tension across membrane receptors with a fluorescent sensor. *Nat. Methods.* **2012**, *9* (1), 64−67.
(29) Liu, Y.; Yehl, K.; Narui, Y.; Salaita, K. Tension sensing nanoparticles for mechano-imaging at the living/nonliving interface. *J. Am. Chem. Soc.* **2013**, *135* (14), 5320−5323.
(30) Zhang, Y.; Ge, C.; Zhu, C.; Salaita, K. DNA-based digital tension probes reveal integrin forces during early cell adhesion. *Nat. Commun.* **2014**, *5* (1), 5167.
(31) Galior, K.; Liu, Y.; Yehl, K.; Vivek, S.; Salaita, K. Titin-Based Nanoparticle Tension Sensors Map High-Magnitude Integrin Forces within Focal Adhesions. *Nano Lett.* **2016**, *16* (1), 341−348.
(32) Blakely, B. L.; Dumelin, C. E.; Trappmann, B.; McGregor, L. M.; Choi, C. K.; Anthony, P. C.; Duesterberg, V. K.; Baker, B. M.; Block, S. M.; Liu, D. R.; Chen, C. S. A DNA-based molecular probe for optically reporting cellular traction forces. *Nat. Methods.* **2014**, *11* (12), 1229−1232.
(33) Morimatsu, M.; Mekhdjian, A. H.; Adhikari, A. S.; Dunn, A. R. Molecular Tension Sensors Report Forces Generated by Single Integrin Molecules in Living Cells. *Nano Lett.* **2013**, *13* (9), 3985−3989.
(34) Zhao, Y. C.; Sarkar, A.; Wang, X. F. Peptide nucleic acid based tension sensor for cellular force imaging with strong DNase resistance. *Biosens. Bioelectron.* **2020**, *150*, 111959.
(35) Zhao, Y.; Pal, K.; Tu, Y.; Wang, X. Cellular Force Nanoscopy with 50 nm Resolution Based on Integrin Molecular Tension Imaging and Localization. *J. Am. Chem. Soc.* **2020**, *142* (15), 6930−6934.
(36) Brockman, J. M.; Su, H. Q.; Blanchard, A. T.; Duan, Y. X.; Meyer, T.; Quach, M. E.; Glazier, R.; Bazrafshan, A.; Bender, R. L.; Kellner, A. V.; Ogasawara, H.; Ma, R.; Schueder, F.; Petrich, B. G.; Jungmann, R.; Li, R. H.; Mattheyses, A. L.; Ke, Y. G.; Salaita, K. Live-cell super-resolved PAINT imaging of piconewton cellular traction forces. *Nat. Methods.* **2020**, *17* (10), 1018−1024.
(37) Chang, Y.; Liu, Z.; Zhang, Y.; Galior, K.; Yang, J.; Salaita, K. A General Approach for Generating Fluorescent Probes to Visualize Piconewton Forces at the Cell Surface. *J. Am. Chem. Soc.* **2016**, *138* (9), 2901−2904.
(38) Ma, R.; Kellner, A. V.; Ma, V. P.-Y.; Su, H.; Deal, B. R.; Brockman, J. M.; Salaita, K. DNA probes that store mechanical information reveal transient piconewton forces applied by T cells. *Proc. Natl. Acad. Sci. U. S. A.* **2019**, *116* (34), 16949−16954.
(39) Ma, V. P. Y.; Hu, Y. S.; Kellner, A. V.; Brockman, J. M.; Velusamy, A.; Blanchard, A. T.; Evavold, B. D.; Alon, R.; Salaita, K. The magnitude of LFA-1/ICAM-1 forces fine-tune TCR-triggered T cell activation. *Sci. Adv.* **2022**, *8* (8), No. eabg4485.
(40) Liu, Y.; Blanchfield, L.; Ma, V. P.; Andargachew, R.; Galior, K.; Liu, Z.; Evavold, B.; Salaita, K. DNA-based nanoparticle tension sensors reveal that T-cell receptors transmit defined pN forces to their antigens for enhanced fidelity. *Proc. Natl. Acad. Sci. U. S. A.* **2016**, *113* (20), 5610−5615.
(41) Zhang, Y.; Qiu, Y. Z.; Blanchard, A. T.; Chang, Y.; Brockman, J. M.; Ma, V. P. Y.; Lam, W. A.; Salaita, K. Platelet integrins exhibit anisotropic mechanosensing and harness piconewton forces to

https://doi.org/10.1021/acsnano.3c07088
ACS Nano 2023, 17, 18584−18595

mediate platelet aggregation. *Proc. Natl. Acad. Sci. U. S. A.* **2018**, *115* (2), 325−330.
(42) Rao, T. C.; Ma, V. P. Y.; Blanchard, A.; Urner, T. M.; Grandhi, S.; Salaita, K.; Mattheyses, A. L. EGFR activation attenuates the mechanical threshold for integrin tension and focal adhesion formation. *J. Cell Sci.* **2020**, *133* (13), jcs238840.
(43) Glazier, R.; Brockman, J. M.; Bartle, E.; Mattheyses, A. L.; Destaing, O.; Salaita, K. DNA mechanotechnology reveals that integrin receptors apply pN forces in podosomes on fluid substrates. *Nat. Commun.* **2019**, *10* (1), 4507.
(44) Wang, L.; Chen, W.; Li, H. Y.; Xiong, C. H.; Sun, F.; Liu, X. Q.; Hu, Y. R.; Wang, W. X.; Zhong, W. Q.; Liu, Z. Exploring Integrin-Mediated Force Transmission during Confined Cell Migration by DNA-Based Tension Probes. *Anal. Chem.* **2022**, *94* (11), 4570−4575.
(45) Luca, V. C.; Kim, B. C.; Ge, C.; Kakuda, S.; Wu, D.; Roein-Peikar, M.; Haltiwanger, R. S.; Zhu, C.; Ha, T.; Garcia, K. C. Notch-Jagged complex structure implicates a catch bond in tuning ligand sensitivity. *Science.* **2017**, *355* (6331), 1320−1324.
(46) Thery, M.; Pepin, A.; Dressaire, E.; Chen, Y.; Bornens, M. Cell distribution of stress fibres in response to the geometry of the adhesive environment. *Cell Motil. Cytoskeleton.* **2006**, *63* (6), 341−355.
(47) Li, H.; Zhang, C.; Hu, Y.; Liu, P.; Sun, F.; Chen, W.; Zhang, X.; Ma, J.; Wang, W.; Wang, L.; Wu, P.; Liu, Z. A reversible shearing DNA probe for visualizing mechanically strong receptors in living cells. *Nat. Cell Biol.* **2021**, *23* (6), 642−651.
(48) Liu, J.; Le, S.; Yao, M.; Huang, W.; Tio, Z.; Zhou, Y.; Yan, J. Tension Gauge Tethers as Tension Threshold and Duration Sensors. *ACS Sensors.* **2023**, *8* (2), 704−711.
(49) Parker, K. K.; Brock, A. L.; Brangwynne, C.; Mannix, R. J.; Wang, N.; Ostuni, E.; Geisse, N. A.; Adams, J. C.; Whitesides, G. M.; Ingber, D. E. Directional control of lamellipodia extension by constraining cell shape and orienting cell tractional forces. *FASEB J.* **2002**, *16* (10), 1195−1204.
(50) Keren, K.; Pincus, Z.; Allen, G. M.; Barnhart, E. L.; Marriott, G.; Mogilner, A.; Theriot, J. A. Mechanism of shape determination in motile cells. *Nature.* **2008**, *453* (7194), 475−480.
(51) Masuda, T.; Baba, K.; Nomura, T.; Tsujita, K.; Murayama, T.; Itoh, T.; Takatani-Nakase, T.; Sokabe, M.; Inagaki, N.; Futaki, S. An influenza-derived membrane tension-modulating peptide regulates cell movement and morphology via actin remodeling. *Commun. Biol.* **2019**, *2* (1), 243.
(52) McMahon, H. T.; Gallop, J. L. Membrane curvature and mechanisms of dynamic cell membrane remodelling. *Nature.* **2005**, *438* (7068), 590−596.
(53) Schiller, H. B.; Hermann, M. R.; Polleux, J.; Vignaud, T.; Zanivan, S.; Friedel, C. C.; Sun, Z.; Raducanu, A.; Gottschalk, K. E.; Thery, M.; Mann, M.; Fassler, R. beta1- and alphav-class integrins cooperate to regulate myosin II during rigidity sensing of fibronectin-based microenvironments. *Nat. Cell Biol.* **2013**, *15* (6), 625−636.
(54) Diaz, C.; Neubauer, S.; Rechenmacher, F.; Kessler, H.; Missirlis, D. Recruitment of alpha(v) beta(3) integrin to alpha(5) beta(1) integrin-induced clusters enables focal adhesion maturation and cell spreading. *J. Cell Sci.* **2020**, *133* (1), jcs232702.
(55) Galbraith, C. G.; Yamada, K. M.; Galbraith, J. A. Polymerizing Actin Fibers Position Integrins Primed to Probe for Adhesion Sites. *Science.* **2007**, *315* (5814), 992−995.
(56) Henson, J. H.; Yeterian, M.; Weeks, R. M.; Medrano, A. E.; Brown, B. L.; Geist, H. L.; Pais, M. D.; Oldenbourg, R.; Shuster, C. B. Arp2/3 complex inhibition radically alters lamellipodial actin architecture, suspended cell shape, and the cell spreading process. *Mol. Biol. Cell* **2015**, *26* (5), 887−900.
(57) Pushkarsky, I.; Tseng, P.; Black, D.; France, B.; Warfe, L.; Koziol-White, C. J.; Jester, W. F.; Trinh, R. K.; Lin, J.; Scumpia, P. O.; Morrison, S. L.; Panettieri, R. A.; Damoiseaux, R.; Di Carlo, D. Elastomeric sensor surfaces for high-throughput single-cell force cytometry. *Nat. Biomed Eng.* **2018**, *2* (2), 124−137.
(58) Galior, K.; Ma, V. P. Y.; Liu, Y.; Su, H. Q.; Baker, N.; Panettieri, R. A.; Wongtrakool, C.; Salaita, K. Molecular Tension Probes to Investigate the Mechanopharmacology of Single Cells: A Step toward Personalized Mechanomedicine. *Adv. Healthc Mater.* **2018**, *7* (14), 1800069.
(59) Piella, J.; Bastus, N. G.; Puntes, V. Size-Controlled Synthesis of Sub-10-nanometer Citrate-Stabilized Gold Nanoparticles and Related Optical Properties. *Chem. Mater.* **2016**, *28* (4), 1066−1075.

https://doi.org/10.1021/acsnano.3c07088
ACS Nano 2023, 17, 18584−18595